# Material Design of Anisotropic Elastic Cellular Bodies with Respect to Contact Problem

**Dorota Jasińska, Małgorzata Janus-Michalska**
*Institute of Structural Mechanics, Cracow University of Technology*
*ul.Warszawska 24, 31-155 Kraków, Poland*
*e-mail: jasinska@limba.wil.pk.edu.pl mjm@limba.wil.pk.edu.pk*

## Abstract

Two-dimensional contact problem formulated for anisotropic, elastic bodies is considered. As an example of anisotropic medium cellular material is taken. The idea of two-scale modeling is adopted for formulation of equivalent continuum, on the basis of which elastic properties can be obtained. (Ref.[2],[3]). Typical cellular microstructures with various types of symmetries are considered. Special attention is paid to cell structures giving negative Poisson's ratio in some directions (re-entrant cells). Application of the energy based criterion for equivalent continuum gives macroscopic yield condition (Ref.[2],[5]). Condition for energy coefficient defined as a sum of weighted energies stored in elastic eigenstates ensures that material works in elastic state. Unilateral frictional contact problem is analyzed using FEM. Calculations are performed for rough contact of square block subjected to normal load. Numerical solutions show differences in deformation type and contact stress distributions for different types of microstructures of analyzed medium. The study enables the optimal choice of material structure topology which ensures the reduction of peak contact pressure and friction stress, and applicability of anisotropic material to the given problem.

*Keywords: contact, friction, cellular anisotropic materials, negative Poisson's ratio*

## 1. Introduction

Cellular materials with their variety of microstructures and types of material symmetries adopted for contact problems provide interesting topic for research. Two scale modeling let us calculate the elastic properties of equivalent continuum on the basis of unit cell analysis. Some cell structures lead to negative Poisson's ratio in some directions. Materials with negative Poisson's ratio are called auxetic due to increasing cross-section in tension. They may be useful for a variety of applications. Among their important mechanical properties the reduction of stress concentration in contact problems shows the new area of applications. Such problem was investigated for auxetic isotropic foam (Ref.[11], [12]) and results show essential differences compared with solutions for conventional foams. For three dimensional isotropic body limits of acceptable Poisson's ratio holds $-1 \le \nu \le 0.5$ as a result of thermodynamical considerations (Ref.[7],[10]). For anisotropic materials these bounds are wider, theoreticaly can reach infinity. The existence of directions with auxetic behaviour in cellular materials is connected with high anisotropy.

## 2. Formulation of the contact problem

For the unilateral static contact problem of anisotropic linear elastic body with stiff and rough obstacle the following system of equations must be fulfilled (Ref.[3]):

$$\sigma_{ij,j} + f_i = 0, \qquad \sigma_{ij} = S_{ijkl}\varepsilon_{kl}, \qquad \varepsilon_{ij} = \frac{1}{2}(u_{i,j} + u_{j,i}) \qquad \text{in } \Omega \tag{2.1}$$

completed with boundary conditions

$$u_i = \hat{u}_i \quad \text{on } \Gamma_D \quad , \qquad \sigma_{ij} \cdot n_j = t_i \quad \text{on} \quad \Gamma_F \tag{2.2}$$

contact conditions on $\Gamma_C$

$$\sigma_n \cdot (u_n - g) = 0, \quad \sigma_n \le 0, \quad u_n - g \le 0 \tag{2.3}$$

and friction conditions on $\Gamma_C$

$$|\boldsymbol{\sigma}_T| < \mu|\sigma_n| \Rightarrow \Delta\mathbf{u}_T = 0, \quad |\boldsymbol{\sigma}_T| = \mu|\sigma_n| \Rightarrow \exists\lambda > 0; \Delta\mathbf{u}_T = -\lambda\boldsymbol{\sigma}_T \tag{2.4}$$

where: $\sigma_{ij}$ - Cauchy stress tensor , $\varepsilon_{ij}$ -small strain tensor, $S_{ijkl}$ - anisotropic elastic stiffness matrix, $u_i$ - displacement vector, $f_i$ -body forces, $\hat{u}_i$ - prescribed displacements on $\Gamma_D$, $t_i$ - forces acting on $\Gamma_F$, $n_i$ -unit normal vector, $\Gamma_D \cup \Gamma_F \cup \Gamma_C$ – boundary of the domain $\Omega$, $g$ - initial gap, $\sigma_n = \sigma_{ij} n_i n_j$ - contact pressure, $u_n = \mathbf{u} \circ \mathbf{n}$ - displacement normal to the boundary, $\sigma_{Ti} = \sigma_{ij} \cdot n_j - \sigma_n \cdot n_i$ - tangential contact force, and $\Delta\mathbf{u}_T = \Delta(\mathbf{u} - u_n \cdot \mathbf{n})$ -increment of tangential displacement.

To solve formulated above boundary value problem (nonlinear due to conditions (2.3) and (2.4)) FEM approach is used.

## 3. Cellular microstructure

Cellular materials due to a variety of material structure topology reveal different anisotropic properties. Microstructure of material is modeled by idealized regular repeating pattern of unit cells. A skeleton of a cell is modeled as elastic beam structure with stiff joints. The following cellular plane structures are analyzed : a) square cell structure, b) 'honeycomb' structure, c) equilateral triangular structure, d) 'reentrant' structure (giving auxetic material). Figure 1 shows mentioned above material structures and their representative unit cells.

a) square cell structure, square unit cell b) 'honeycomb' structure, triangle unit cell

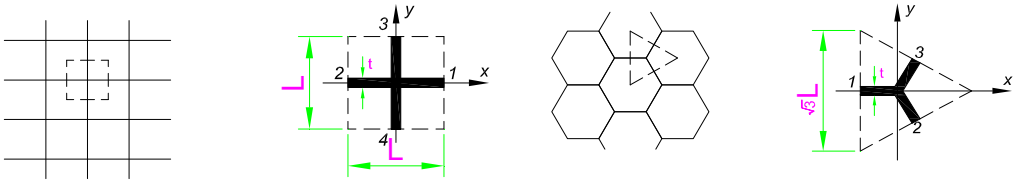


c) equilateral triangular structure, hexagonal unit cell d) 'reentrant' structure, trapezoid unit cell

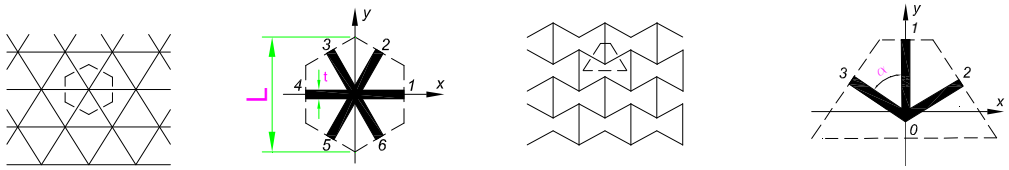


Fig. 1. Regular cellular plane structures, and their representative unit cells.

Geometry of representative unit cell can be described by midpoint position vectors: $\mathbf{b}_i^0$, where: $\left|\mathbf{b}_1^0\right| = h/2$ , $\left|\mathbf{b}_i^0\right| = L/2$, $i = 1,2,...n$ . L, h, t, γ - geometric structural parameters (for a, b, c structures $L = h$). Skeleton material parameters are: Young modulus - $E_s$ ,Poisson's ratio - $\nu_s$ , limit of linear elasticity- $R_e$ .

### 3.1 Stiffness matrices

A framework of micromechanical modeling (Ref.[2], [3],[5]). is used to obtain stiffness matrices of elastic anisotropic equivalent continuum. It starts with analyzing strains defined as follows:

$$\boldsymbol{\varepsilon} = \left\langle \boldsymbol{\varepsilon}^s \right\rangle_V = \frac{1}{V} \sum_{A_i} sym\left(\mathbf{n}_i \otimes \mathbf{u}_i\right) dS \tag{3.1}$$

where: $\mathbf{u}_i$ midpoint displacement vector,

$\mathbf{n}_i$ unit normal to the cell boundary.

Given uniform strain field ${}^K\tilde{\varepsilon}$ , $K = 1,2,3$ on the unit cell, the displacements for the midpoints $i = 1,2,...n$ in skeleton structure can be found :

$$\boldsymbol{\Delta}_i = \boldsymbol{\Delta}_i\left({}^K\tilde{\varepsilon}\right) \qquad i = 1,2,...n\,, \qquad K = 1,2,3 \tag{3.2}$$

Next the resultant forces

$${}^K\tilde{F}_{in} = \tilde{F}_{in}\left({}^K\varepsilon\right), \quad {}^K\tilde{F}_{i\tau} = \tilde{F}_{i\tau}\left({}^K\varepsilon\right) \qquad i = 1,2,...n \qquad K = 1,2,3 \tag{3.3}$$

in skeleton beams are obtained. In a, b, c) structure analytical solutions obtained in Mathcad program is used. In d) as a result of numerical solution – FEM code (ANSYS).

For arbitrary uniform strain state ${}^K\varepsilon$ the forces can be calculated as linear combination of previous solutions and reads as follows:

$$F_{in}\left({}^K\varepsilon\right) = \sum_{K=1}^{3} {}^K\varepsilon \; {}^K\tilde{F}_{in}\,, \qquad F_{i\tau}\left({}^K\varepsilon\right) = \sum_{K=1}^{3} {}^K\varepsilon \; {}^K\tilde{F}_{i\tau} \tag{3.4}$$

For the resultant forces stress tensor $\boldsymbol{\sigma}^s$ in each point of beam skeleton structure can be obtained.

Stresses for equivalent continuum for structures a, b, c are based on micromechanical definition of averaging of stress field for skeleton [3]:

$$\boldsymbol{\sigma} = \left\langle \boldsymbol{\sigma}^s \right\rangle_V = \frac{1}{V} \int_{V_s} \boldsymbol{\sigma}^s dV_s \tag{3.5}$$

Stiffness matrices $\mathbf{S}$ can be derived by the use of linear relation $\boldsymbol{\sigma} = \mathbf{S} : \boldsymbol{\varepsilon}$

For structures a, b, c, stiffness matrices components are given by analytical formulae in dependence on microstructural geometric and skeleton material parameters (Appendix 1).

For structure d) definition of equivalent continuum is based on averaging of strain potential for skeleton Ref.[2] as written below:

$$\Phi_E = \frac{1}{V} \int_{V_s} {}^s\Phi_E dV_s \tag{3.6}$$

which gives the following stiffness matrix components for equivalent continuum

$$S_{IJ} = \frac{1}{V} \left( \frac{\int_{V_s} \partial^2 {}^s\Phi_E}{\partial\left({}^I\varepsilon\right) \; \partial\left({}^J\varepsilon\right)} \right) \tag{3.7}$$

These components can be obtained as a result of numerical procedure based on equations (3.1)-(3.4) and (3.6)-(3.7) (Ref.[2]).

### 3.2 Poisson's ratio and other material properties

Typical cellular structures with honeycomb, and triangle shape of skeleton give always positive Poisson's ratio values in each direction in plane since they represent transversal symmetry. For isotropy in two-dimensional problems limits of acceptable Poisson's ratio become $-1 \le \nu \le 1$ due to thermodynamical considerations (Ref.[9]). The honeycomb structure is more compliant and Poisson's ratio can attain greater value but limited by relation $\nu \le 1$. The triangular structure shape is stiff and gives lower Poisson's ratio. The value of Poisson's ratio for the symmetries mentioned above is constant; it means that it is independent on direction of tension. This constant is dependent on geometric and material microstructural parameters as given in Appendix 2. Square structure gives anisotropic material with zero Poisson's ratio in symmetry axis. In other directions the value is limited by relation $0 \le \nu \le 1$. Generally for greater cellular material density of fixed microstructure type the Poisson's ratio value is lower than for lower density. Some skeleton geometries lead to nonpositive Poisson's ratio. For instance honeycomb with inverted hexagonal cells, leads to negative Poisson's ratio in some directions .This unusual characteristic is achieved by forming the cells into re-entrant shape, which bulges inwards and which unfolds under tension resulting in a lateral expansion (Ref.[6]). Detailed study of directional properties of cellular material with re-entrant honeycomb structure in dependence on microstructural parameters is given in Ref.[2].
Graphical representation of chosen material properties for material structures a, b, c, d with geometric and skeleton material data used for numerical examples are given in Appendix 2.
Evaluation of cellular material properties decides on the applicability of the material to the given problem.

### 3.3 Assessment of elastic range

Majority of cellular materials reveal nonlinear behavior. Although linear analysis gives only estimation of elastic limits it enables to predict applicability of chosen microstructure to material design.
Matrix representation of stiffness tensor for plane structures in Kelvin's notation in 6-D space is as follows:

$$\mathbf{S} = \begin{bmatrix} S_{11} & S_{12} & S_{13} \\ S_{12} & S_{22} & S_{23} \\ S_{13} & S_{23} & S_{33} \end{bmatrix} \tag{3.8}$$

In general this matrix has three eigenvalues: $\lambda_{\mathrm{I}}, \lambda_{\mathrm{II}}, \lambda_{\mathrm{III}}$
and corresponding stiffness matrix eigenstrains:
$^{\mathrm{I}}\tilde{\boldsymbol{\varepsilon}} = \left( {}^{\mathrm{I}}\tilde{\varepsilon}_x, {}^{\mathrm{I}}\tilde{\varepsilon}_y, {}^{\mathrm{I}}\tilde{\varepsilon}_{xy} \right), {}^{\mathrm{II}}\tilde{\boldsymbol{\varepsilon}} = \left( {}^{\mathrm{II}}\tilde{\varepsilon}_x, {}^{\mathrm{II}}\tilde{\varepsilon}_y, {}^{\mathrm{II}}\tilde{\varepsilon}_{xy} \right), {}^{\mathrm{III}}\tilde{\boldsymbol{\varepsilon}} = \left( {}^{\mathrm{III}}\tilde{\varepsilon}_x, {}^{\mathrm{III}}\tilde{\varepsilon}_y, {}^{\mathrm{III}}\tilde{\varepsilon}_{xy} \right)$
or stiffness matrix eigenstress:

$$^{\mathrm{I}}\tilde{\boldsymbol{\sigma}} = \lambda_{\mathrm{I}}\, {}^{\mathrm{I}}\tilde{\boldsymbol{\varepsilon}} \;,\; {}^{\mathrm{II}}\tilde{\boldsymbol{\sigma}} = \lambda_{\mathrm{II}}\, {}^{\mathrm{II}}\tilde{\boldsymbol{\varepsilon}},\; {}^{\mathrm{III}}\tilde{\boldsymbol{\sigma}} = \lambda_{\mathrm{III}}\, {}^{\mathrm{III}}\tilde{\boldsymbol{\varepsilon}}. \tag{3.9}$$

Equations (3.1)-(3.4) enable to calculate forces in skeleton structure for strain eigenstates and formulate the limit condition for bending and tension in skeleton in the form:

$$\max_i \left( {}^{\alpha}\sigma_x^s \right) = R_e \qquad \alpha = \text{I,II,III} \qquad i = 1, 2, ...n \tag{3.10}$$

The coefficients defined as follows**:**

$$k_\alpha := \frac{R_e}{{}^{\alpha}\tilde{\sigma}_x^s} \qquad \alpha = \text{I,II,III} \tag{3.11}$$

are obtained as a result of analytical considerations or numerical calculations. Analytical formulae for these coefficients in dependence on geometric structural and skeleton material parameters for structures a, b, c are given in Appendix 1. For structure d these coefficient are obtained as a result of numerical calculations.
Limit eigenstrains and eigenstresses are as follows:

$${}^{\alpha}\boldsymbol{\varepsilon}^{\text{gr}} = k_\alpha \, {}^{\alpha}\tilde{\boldsymbol{\varepsilon}} \ , \quad {}^{\alpha}\boldsymbol{\sigma}^{\text{gr}} = \lambda_\alpha \, {}^{\alpha}\boldsymbol{\varepsilon}^{\text{gr}}, \ \ \alpha = \text{I,II,III} \, . \tag{3.12}$$

The analysis presented above let us also predict deformability of given material in elastic range. It can be described as maximum elongation in x, y direction or shear angle in the xy plane, which reads as follows:

$$\max \left| \varepsilon_x \right| = \sum_{\alpha=1}^{\text{III}} \left| {}^{\alpha}\varepsilon_x^{\text{gr}} \right| \quad , \quad \max \left| \varepsilon_y \right| = \sum_{\alpha=1}^{\text{III}} \left| {}^{\alpha}\varepsilon_y^{\text{gr}} \right| , \quad \max \left| \varepsilon_{xy} \right| = \sum_{\alpha=1}^{\text{III}} \left| {}^{\alpha}\varepsilon_{xy}^{\text{gr}} \right| \, . \tag{3.13}.$$

### 3.4 Energy based yield criterion for anisotropic continuum

For arbitrary anisotropic solid energy based Rychlewski criterion (Ref.[13]) is formulated in the form of sum of weighted energies stored in eigenstates of anisotropy stiffness tensor and is as follows:

$$\sum_{\alpha=1}^{\text{III}} \frac{{}^{\alpha}\Phi_E}{{}^{\alpha}\Phi_E^{\text{gr}}} = 1 \tag{3.14}$$

where: ${}^{\alpha}\Phi_E^{\text{gr}}$ is the critical energy for $\alpha$ state, $\alpha = \text{I,II,III}$**.**
Energy based yield criterion is a type of energy hypothesis for cellular material. The subject of investigation is the limit state of linear elasticity which corresponds to the first yield point in the skeleton structure. Such an approach was successively adopted to cellular 3D structured material (Ref. [3],[5]) and foams. It shows good agreement with experimental data (Ref. [5]).
Critical energies in eq. (3.14) can be calculated by the use of formula:

$${}^{\alpha}\Phi_E^{\text{gr}} = \frac{1}{2} \, {}^{\alpha}\boldsymbol{\sigma}^{\text{gr}} \cdot {}^{\alpha}\boldsymbol{\varepsilon}^{\text{gr}} = \frac{1}{2} \lambda_\alpha \, k_\alpha^2 \, {}^{\alpha}\tilde{\boldsymbol{\varepsilon}} \tag{3.15}$$

The criterion presented above gives macroscopic yield condition for arbitrary stress state. In particular for uniaxial tension, which is important due to the fact that it can be compared with experimental results. For the considered structures a), b), c) formulae in dependence on skeleton material parameters and geometric parameters of skeleton structures are given in Appendix 1. For structure d) these energies are obtained numerically.

The elastic stiffness matrix (3.8), yield stresses, and limit strains (3.12), (3.13) describing deformability in the elastic range depend on material properties of a solid phase of the cell, and topological arrangement of it's structure. Detailed study of material properties in relation with structural parameters is given in Ref. [2], [3].

### 3.5. Material effort in arbitrary plane stress state

The considered contact problem is linearly elastic. To conform this requirement it is necessary to introduce a measure of material effort in arbitrary point of material and give the range of this measure for elasticity. The consequence of adopted form of yield criterion is the choice of energy coefficient defined as a sum of weighted energies stored in subsequent eigenstates as written below:

$$\varphi = \sum_{\alpha=1}^{\mathrm{III}} \frac{{}^{\alpha}\Phi_E}{{}^{\alpha}\Phi_E^{\mathrm{gr}}} \tag{3.16}$$

In limit state the coefficient reaches its maximum value $\varphi = 1$.

Critical energies can be defined as structural parameters of material effort.

For generality of considerations we assume arbitrary orientation of cellular x, y axes to global X,Y coordinate axes in which contact problem is described. This orientation can be given by β angle as shown in Fig 2.

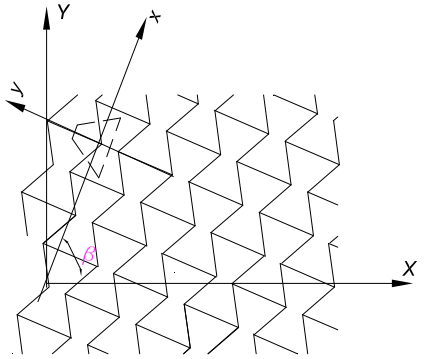


Fig. 2. Material orientation with respect to global coordinate system.

To evaluate energy coefficient in arbitrary M point with stress vector:

$$\boldsymbol{\sigma}^{(M)} = \left(\sigma_X^{(M)}, \sigma_Y^{(M)}, \sqrt{2}\sigma_{XY}^{(M)}\right) \tag{3.17}$$

it is necessary to decompose it into stress eigenstates. As a result stress vector for M point can be expressed as linear combination of limit eigenstresses as written below:

$$\boldsymbol{\sigma}^{(M)} = A\ {}^{\mathrm{I}}\boldsymbol{\sigma}^{\mathrm{gr}} + B\ {}^{\mathrm{II}}\boldsymbol{\sigma}^{\mathrm{gr}} + C\ {}^{\mathrm{III}}\boldsymbol{\sigma}^{\mathrm{gr}} \tag{3.18}$$

where coefficients of this combination are as follows:

$$A = \frac{\sigma_X^{(M)}\ {}^{\mathrm{II}}\sigma_Y^{\mathrm{gr}} - \sigma_Y^{(M)}\ {}^{\mathrm{II}}\sigma_X^{\mathrm{gr}}}{{}^{\mathrm{I}}\sigma_X^{\mathrm{gr}}\ {}^{\mathrm{II}}\sigma_Y^{\mathrm{gr}} - {}^{\mathrm{II}}\sigma_X^{\mathrm{gr}}\ {}^{\mathrm{I}}\sigma_Y^{\mathrm{gr}}},\quad B = \frac{\sigma_Y^{(M)}\ {}^{\mathrm{I}}\sigma_X^{\mathrm{gr}} - \sigma_X^{(M)}\ {}^{\mathrm{I}}\sigma_Y^{\mathrm{gr}}}{{}^{\mathrm{I}}\sigma_X^{\mathrm{gr}}\ {}^{\mathrm{II}}\sigma_Y^{\mathrm{gr}} - {}^{\mathrm{II}}\sigma_X^{\mathrm{gr}}\ {}^{\mathrm{I}}\sigma_Y^{\mathrm{gr}}},\quad C = \frac{\sigma_{XY}^{(M)}}{{}^{\mathrm{III}}\sigma_{XY}^{\mathrm{gr}}}. \tag{3.19}$$

The energy coefficient is expressed by relation:

$\varphi = A^2 + B^2 + C^2 \le 1$

which gives the following condition: (3.20)

$$\varphi = d_1\left(\sigma_X^{(M)}\right)^2 + d_2\left(\sigma_Y^{(M)}\right)^2 + d_3\left(\sigma_{XY}^{(M)}\right)^2 + d_4\left(\sigma_X^{(M)}\sigma_Y^{(M)}\right) + d_5\left(\sigma_X^{(M)}\sigma_{XY}^{(M)}\right) + d_6\left(\sigma_Y^{(M)}\sigma_{XY}^{(M)}\right) \le 1$$

where:

$$d_1 = 0.25\left[\left(\frac{1}{m_1}\right)^2 + \left(\frac{\cos 2\beta}{m_2}\right)^2 + \left(\frac{\sin 2\beta}{m_3}\right)^2\right],\qquad d_1 = d_2,\qquad d_3 = \left[\left(\frac{\sin 2\beta}{m_2}\right)^2 + \left(\frac{\cos 2\beta}{m_3}\right)^2\right],$$

$$d_4 = 0.5\left[\left(\frac{1}{m_1}\right)^2 - \left(\frac{\cos 2\beta}{m_2}\right)^2 - \left(\frac{\sin 2\beta}{m_3}\right)^2\right],\quad d_5 = 0.5\sin 4\beta\left[\left(\frac{1}{m_2}\right)^2 + \left(\frac{1}{m_3}\right)^2\right],\quad d_6 = -d_5$$

$$m_1 = \lambda_1 k_1,\quad m_2 = \lambda_2 k_2,\qquad m_3 = \lambda_3 k_3 \big/ \sqrt{2}.$$

and $\beta$ is the angle shown in Fig.2

## 4. Numerical analysis

Calculations of stiffness matrices and energy effort material parameters for considered anisotropic materials are performed independently on microstructural level by considering strain stress relations for unit cell. Analytical formulae for stiffness matrices coefficients and critical energies for structures a), b), c) are obtained with application of symbolic operations provided by Mathcad program. For structure d) relevant description can be obtained numerically by the use of FEM system.

Subsequently those parameters were used in FEM analysis (with ANSYS software) of numerical examples presented below.

All examples deal with rectangular prism in plane state of strain, in rough contact with stiff flat foundation Simple geometry and load enable to analyze the influence of microstructure type on deformation, contact stresses and distribution of material effort coefficient.

### *4.1 Square block made of material with different cell types under pressure*

A square block of dimensions B*H=1*1m in contact with stiff foundation is analysed. Contact is rough with coefficient of friction μ=0.3. Pressure p=25kN/m is applied to upper edge of the block (see Fig. 3).

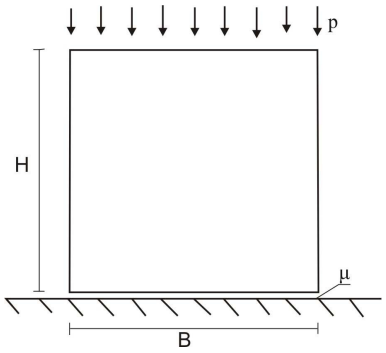


Fig. 3. Geometry and load for numerical examples.

Materials of all presented above types of microstructure are considered. Skeleton material data are: $E_S$=10GPa, $\nu_S$=0.3, $R_e$=10MPa and the geometric parameters are chosen to obtain the same relative material density ρ=0.1154 of anisotropic cellular media in all cases. Table 1. shows specification of geometrical parameters for unit cells. Notation for types of microstructures are the same as in Fig.1.

Table 1. Specification of unit cells

| Structure type | Geometric parameters of skeleton [mm] | Skeleton beam thickness t [mm] |
|---|---|---|
| a) | $L_{01}=L_{02}=L_{03}=L_{04}=2.6$ | 0.15 |
| b) | $L_{01}=L_{02}=L_{03}=L_{04}=L_{05}=L_{06}=1.5$ | 0.15 |
| c) | $L_{01}=L_{02}=L_{03}=4.5$ | 0.15 |
| d) | $L_{01}=L_{02}=L_{03}=3.15$ $\gamma=70^0$ | 0.15 |

Resultant macroscopic material constants are put together in Table 2.

Table 2. Anisotropic material constants for cellular materials of different cell types.

| Structure type | $E_X$ [MPa] | $E_Y$ [MPa] | $\nu_{XY}$ | $\nu_{YX}$ |
|---|---|---|---|---|
| a) $\beta = 0$ | 576.92 | 576.92 | 0.0 | 0.0 |
| b) | 21.87 | 21.87 | 0.96 | 0.96 |
| c) | 385.47 | 385.47 | 0.33 | 0.33 |
| d) $\beta=90^o$ | 0.13 | 1.95 | -0.26 | -3.85 |

Analysis of Table 2. leads to the conclusion that macroscopic material constants highly depend on type of cellular structure. Resultant Young moduli are the biggest for structures a) and c), smaller for honeycomb structure b) and several orders smaller for re-entrant structure d). Materials of structures b) and c) are isotropic and have positive Poisson's ratio. Material of structure a) has zero Poisson's ratios and structure d) produces negative Poisson's ratios, when unit cell axis are placed parallel to coordinate frame.

Contact problem with application of described cellular solids is solved. Figure 4 shows deformations of square block for different materials.

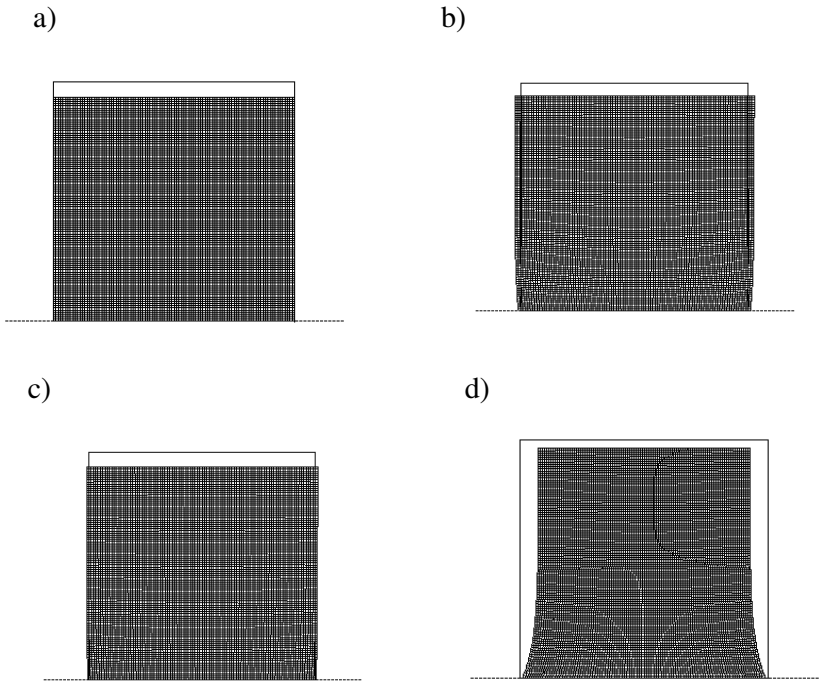


Fig. 4. Deformation of square block of cellular material, a) square cell (material: a) displacement scale 1500, b) honeycomb cell (material b) displacement scale 50, c) triangle (material c) displacement scale 1000, d) re-entrant (material d) displacement scale 3.

Differences in deformation types for structures with positive, zero, and negative Poisson's ratio can be observed.

Figures 5 and 6, show relative contact pressure, friction stress distribution, and contact status along contact line.

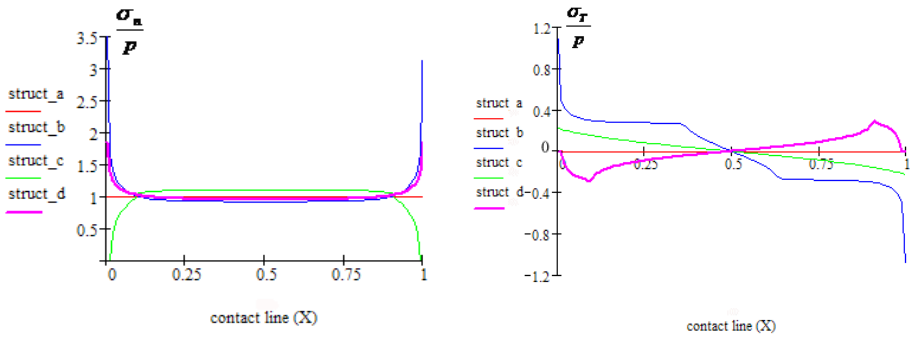


Fig.5. Contact pressure and friction stress distribution along contact line for different cell types.

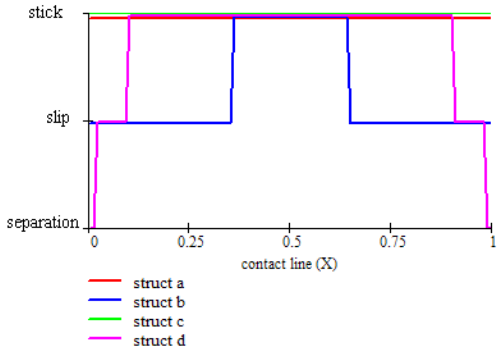


Fig. 6. Contact status (stick slip and separation zones) for different cell types.

It can be clearly seen from Fig. 5 that the most advantageous contact stress distributions correspond to material with nonpositive Poisson's ratio. For material a) characterized by $\nu_{XY}=0$, contact pressure is constant and friction stress vanishes. For structure d) with $\nu_{XY}<0$ contact pressure is homogenous in the centre of contact zone, and decreasing near the edges. Friction stress maximum appears at the point where slip begins. Fig. 6 shows contact separation at the corners for this material. Structures b) and c), characterized by positive, constant ν, show well known pick contact pressure and friction force at the corners of the contact zone. This concentration is much greater for structure b) with ν as big as 0.96 in comparison to material with c) structure where ν attains the value 0.3.

During calculations energy based yield criterion (3.20) is checked to ensure work in elastic range . Distribution of material effort coefficient for materials with structures b), c), and d) are shown in Fig.7. For material with structure a) the value of this coefficient is constant (φ=1.0E-5). Vanishing of Poisson's ratio results in the lack of friction in this load case. For structures with positive Poisson's ratio material effort coefficient reaches maximum value in the corners of contact surface as a result of peak contact pressure. Points with maximum coefficient for structure d) correspond with maximum friction force. Reduction of the material effort in the

center of contact area for structures b) and d) can be explained by energy considerations in microscale.

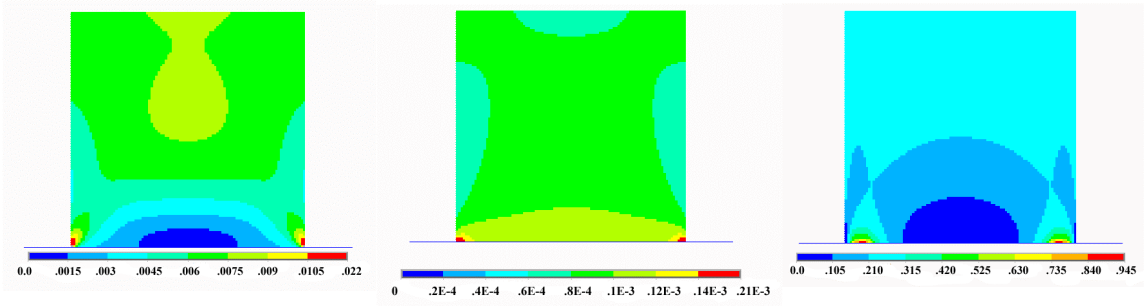


Fig. 7. Distribution of material effort coefficient for material of structures b), c), d).

For the considered cellular materials results of numerical calculations are summarised in Table 3. The last column of this table presents the ratio of applied pressure to admissible vertical load in nonfrictional case ($p_{ymax}$) for estimation of applicability of chosen material to given contact problem.

Table 3. Results for different cell types

| Structure type | $\sigma_{n\,max}/p$ | $\sigma_{t\,max}/p$ | $\varphi_{max}$ | $p/p_{ymax}$ |
|---|---|---|---|---|
| a) | 1 | 0 | 0.00001 | 0.004 |
| b) | 3.6 | 1.08 | 0.022 | 0.083 |
| c) | 1.85 | 0.23 | 0.0002 | 0.009 |
| d) | 1.09 | 0.28 | 0.95 | 0.492 |

*4.2. Square block made of re-entrant cellular material with different location of cell axis with respect to contact line.*

Square block with geometry and contact data as in example 4.1 with pressure p=4 kN/m applied to it's upper edge is analyzed. The block is made of re-entrant cell structure d) with skeleton material data and geometry of the unit cell as in Table 1, but with different placing of the cell symmetry axis with respect to global coordinate system (and subsequently to body geometry, load and contact line). Calculations were made for three chosen angle values: 0, 45, and 90 degree (see Fig. 2). Macroscopic, anisotropic material constants for those cases are presented in Table 4.

Numerical results are visualized in Fig. 8-11. The greatest vertical load capacity and the smallest Poisson's ratio $\nu_{YX=}$-3.85 correspond to the angle 90 degree. It causes the reduction of contact pressure, and hence friction stress near the ends of contact line with separation at the corners. The more uniform contact pressure distribution appears for the angle 0 degree, with negative, but smaller absolute value Poisson's ratio $\nu_{XY} = -0.26$. The skew placement of the cell results in positive Poisson's ratio, peak contact stresses at the corners, and unsymmetric deformation despite symmetric boundary conditions due to lack of symmetry in

microstructure. For 90 degree angle despite smallest $\nu_{YX=}$-3.85, the stick area dominates in contact zone (Fig. 9). It is caused by domination of resultant shear modulus over bulk modulus. Directional proportion G/K reveals dilatational properties of the considered material and determines relation of shear and dilatational deformation. For 0 degree more uniform deformation (Fig. 10), and predominance of slip in contact area (Fig. 9) is observed. Distributions of material effort coefficient is presented in Fig. 11. In all cases reduction of material effort can be noticed in the center of contact zone. It can be explained by considerations on a microscale level.

Table 4 . Anisotropic material constants for different β angles.

| β | $E_X$ [MPa] | $E_Y$ [MPa] | $\nu_{XY}$ | $\nu_{YX}$ | $p/p_{ymax}$ |
|---|---|---|---|---|---|
| 0 | 1.954 | 0.128 | -3.85 | -0.26 | 0.31 |
| 45 | 0.104 | 0.104 | 0.365 | 0.365 | 0.38 |
| 90 | 0.128 | 1.954 | -0.26 | -3.85 | 0.08 |

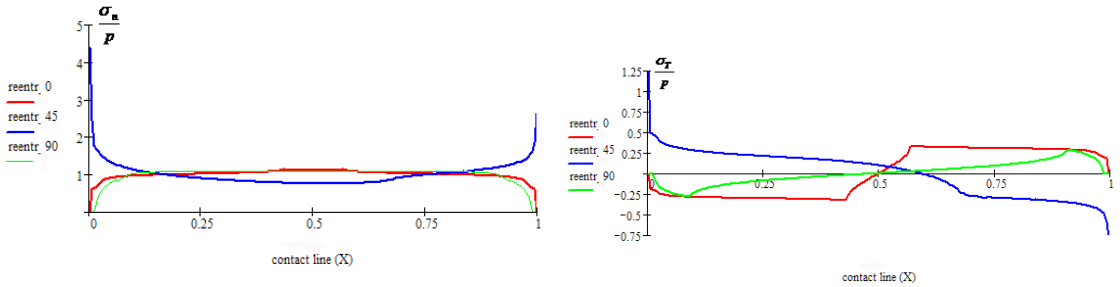


Fig. 8. Contact pressure and friction stress distribution along contact line for different reentrant cell orientation

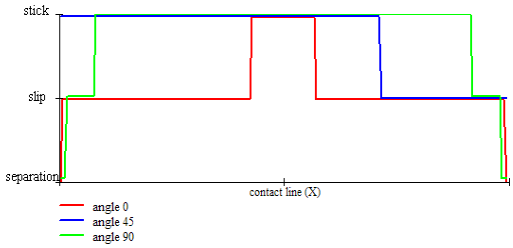


Fig. 9. Contact status (stick, slip, and separation zones) for different re-entrant cell orientation

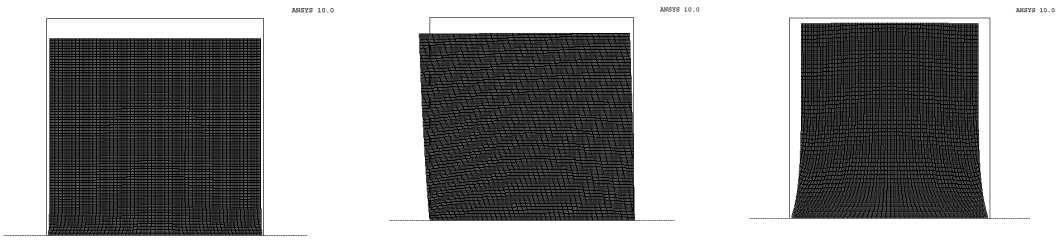

Fig. 10. Deformation of square block made of reentrant cell microstructure for different cell orientation: β=0 deformation scale 3, β=45 deformation scale 2, and β=90 deformation scale 15.

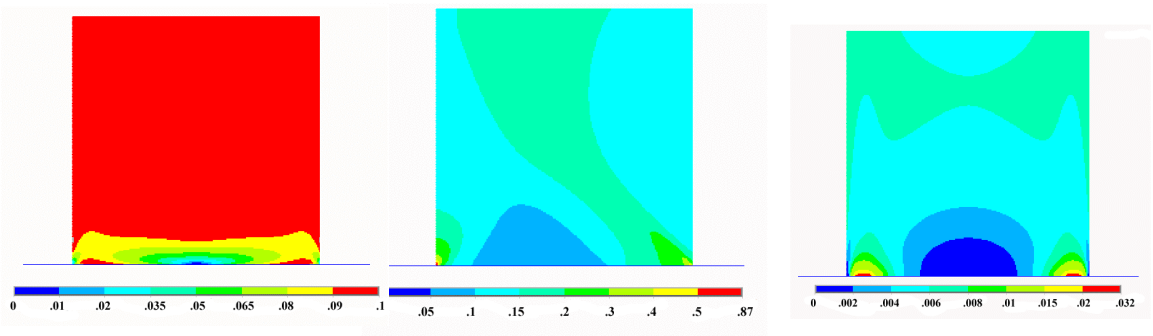


Fig. 11. Distribution of material effort coefficient for different reentrant microstructure orientation: β=0, β=45, and β=90.

*4.3. Square block made material of square cells with different location of cell axis with respect to contact line*

For comparison to the previous example the block with the same geometry, load and boundary conditions, but made of material with structure a) (square cell) with different orientation of cell symmetry axis with respect to global coordinate system is considered. Chosen angle values are: 0 and 45 degree (due to structure symmetry results for 0 and 90 degree agree ).

Material constants are given in Table 5.

Table 5. Anisotropic material constants for different β angles.

| β | $E_X$ [MPa] | $E_Y$ [MPa] | $\nu_{XY}$ | $\nu_{YX}$ | $p_y/p_{ymax}$ |
|---|---|---|---|---|---|
| 0 | 576.92 | 576.92 | 0 | 0 | 0.0005 |
| 45 | 3.795 | 3.795 | 0.99 | 0.99 | 0.018 |

Figures 12-15 present results of numerical calculations

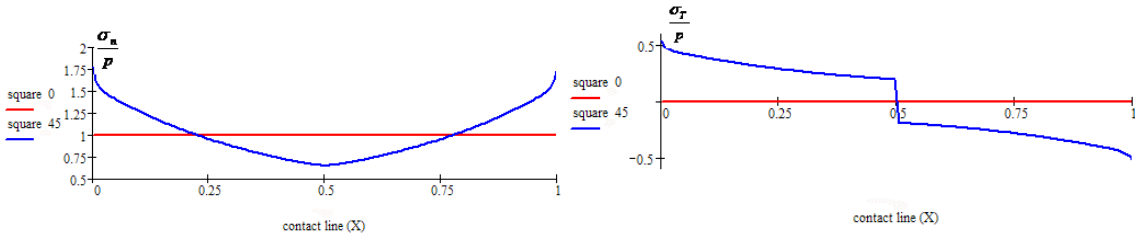


Fig.12. Relative contact pressure and friction stresses distribution along contact line for different square cell orientation.

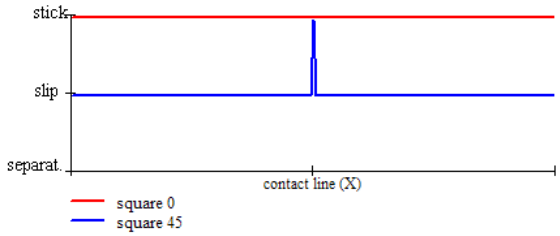


Fig. 13. Contact status (stick, slip, and separation zones) for different square cell orientation.

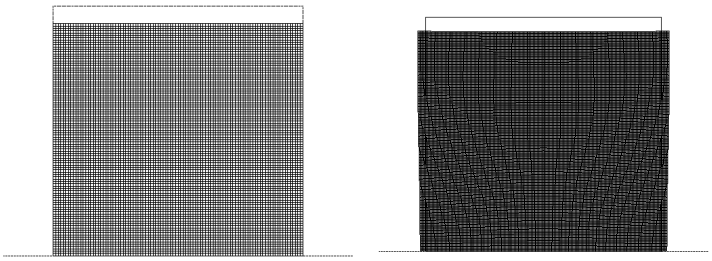

Fig. 14. Deformation of the body for different square cell orientation: β=0 deformation scale 10000, β=45 deformation scale 50.

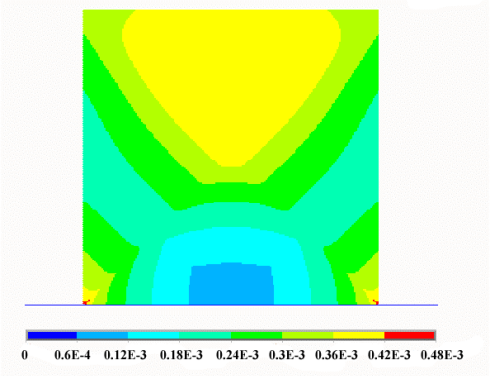


Fig.15. Distribution of material effort coefficient for square cell structure with orientation: β=45.

Skew placement of the cell (β=45) resulting in high positive Poisson's ratio leads to peak of normal and tangential contact stresses (Fig. 12, 13), and concentration of material effort (fig. 15) in the corners of the contact line. Directions of reduction of material effort for this case correspond with maximum stiffness directions (see Appendix 2). Unlike for the re-entrant cell in example 4.2 deformation in this case is symmetrical, due to square structure symmetry for 45 degree. For material orientation given by β=0 ($\nu_{XY}=\nu_{YX}=0$) contact pressure is constant, friction stress equals zero, and material effort is uniform. The value of the material effort coefficient is: φ= 2.5E-7.

Detailed comparison of results of numerical examples presented above shows that stress field and contact status depend on macroscopic material properties, especially on Poisson's ratio. This ratio for cellular materials depends mainly on topology of microstructure. Analysed structures of types b) and c) give isotropic material with positive Poisson's ratio and hence high peak contact pressure and friction stresses.

Structure d) (re-entrant ) gives compliant material with negative Poisson's ratios for broad range of angles ($\beta \in (-18^o, 18^o) \cup (72^o, 108^o)$) (see Appendix 2d.). So the assumption that deformation at small strains does not influence material properties can be adopted in this case. Such material with proper placement with respect to contact line can produce advantageous contact pressure distributions with reductions in the corners of contact area.

Structure a) with cell symmetry axis parallel to contact line, gives very stiff material with zero Poisson's ratio. It might seem to be the most advantageous for the class of contact problems presented above (with loads perpendicular to contact line and hence without global sliding), because it produces uniform contact pressure and zero friction stress. However it is worth to notice that material of structure a) has zero Poisson's ratio, only for unit cell placed exactly parallel to coordinate frame. Graph of dependence of $\nu_{XY}$ on the angle of cell orientation shows that for all angles other than 0 and 90 the Poisson's ratio is positive, and can reach high value, even in the close neighbourhood of 0 and 90 (see Appendix 2a.) The assumption, typical for linear analysis, that initial configuration of the structure is reference configuration may be inappropriate in this case. It may cause that advantageous properties of the material can be overestimated. Real contact properties especially for materials with Poisson's ratio very sensitive to cell orientation should be obtained as a result of full nonlinear analysis, in which anisotropic effective properties of material are dependent on local configuration of deformed body.

## 5. Conclusions

An analysis of static contact of cellular solid with rough stiff foundation is undertaken. Micromechanical model of cellular material is applied to predict mechanical properties on a macroscale. The study is focused on prediction of stress distribution in contact zone and material effort in the elastic range. Cellular materials due to a variety of structure topology, which results in different types of material symmetry and macroscopic properties can be tailored to special demands of the given problem. The example of contact shows that differences in behaviour can be essential and clearly visible. Special attention is paid to materials with anisotropic properties especially to materials with re-entrant structure, which give negative Poisson's ratio in a certain range of directions. Proper choice of microstructural geometrical parameters can determine expected elastic properties. This properties and orientation of material symmetry axis with respect to load direction can significantly influence contact stress distribution and may play an important role in reducing contact peak pressure. Comparison of material with square cells with material of re-entrant structure allows to point out more advantageous type of microstructure by discussion of influence of directional material properties on results of given example.

The contact mechanics of cellular materials is important to their friction and wear behaviour and also, under static conditions in applications as antivibrating supports. The first topic requires consideration on a microscale and with two-scale modelling approach can be promising area for research. The second topic requires analysis on a macro scale. The work on this problem started in this paper can be developed.

## 6. References


[1] ANSYS 10.0 manual

[2] Janus-Michalska M., Energy Based Approach Constructing Elastic Model of Auxetic Cellular Materials, in preparation for *The 1st Congress of Mechanics*, Warsaw VIII 2007.

[3] Janus-Michalska M., Effective Models Describing Elastic Behaviour of Cellular Materials, *Archives of Metallurgy and Materials,* vol.50, issue 3,pp.595-608, 2005.

[4] Kikuchi N., Oden J.T., *Contact Problems in Elasticity: A study of Variational Ineqalitiees and Finite Element Methods*, SIAM Philadelphia, 1988.

[5] Kordzikowski P., Janus-Michalska M., Pęcherski R.B., Specification of Energy –Based Criterion of Elastic Limit States for Cellular Materials, *Archives of Metallurgy and Materials,* vol.50, issue 3, pp. 621-634, 2005.

[6 ] Lakes, R.S., Foam structures with a negative Poisson's ratio, *Science,* 235, pp.1038–1040, 1987.

[7] Lakes, R.S., Design considerations for materials with negative Poisson's ratios, *Trans. ASME J. Mech.* 115, pp. 696–700, 1993.

[8] Overaker D.W., Cuitino A.M., Langrana N.A., Elastoplastic Micromechanical Modeling of Two-dimensional Irregular Convex and Nonconvex (Re-entrant) Hexagonal Foams, *Transactions of ASME*, 65, 1998.

[9] Scalia A., Contact Problem for Porous Elastic Half-Plane, *J. Elasticity*, vol.60, pp.91-102,2000.

[10] Stavroulakis G.E., Auxetic behavior: appearance and engineering applications, *Physica Status Solidi,* No. 3, pp.710-720, 2005.

[11] Szefer G., Kędzior D., Contact of Elastic Bodies with Negative Poisson's Ratio, Springer V., 2002.

[12] Wang Y., Lakes R., Analytical parametric analysis of the contact problem of human buttocks and negative Poisson's ratio foam cushions, *Int.J.Sol.Struc.* 39, pp. 4825-38, 2002.

[13] J.Rychlewski, Unconventional approach to linear elasticity, *Arch. Mech.*, 47, pp.149-171. (1995).


## 7. Appendix 1.

**Stiffness matrices, Kelvin moduli, eigenstates and critical energies.**

Notation: $\mathbf{S}$ – stiffness matrix, $\lambda_\alpha$ – eigenvalues of $\mathbf{S}$, ${}^{\alpha}\tilde{\boldsymbol{\varepsilon}}$-strain eigenstates, $k_\alpha$-scalar multiplier for critical eigenstate, ${}^{\alpha}\Phi_E^{\mathrm{gr}}$ - critical energies in eigenstates, α=I, II, III.

L, h, t, γ – microstructural parameters (Fig. 1),

$E_s$, $v_s$, $R_e$ – skeleton material parameters.

a) Square cell structure

$$\mathbf{S} = \begin{bmatrix} \frac{E_s t}{L} & 0 & 0 \\ 0 & \frac{E_s t}{L} & 0 \\ 0 & 0 & \frac{E_s t^3}{L^3} \end{bmatrix}$$

$$\lambda_{\text{I}} = \frac{E_s t}{2l_i},\ \lambda_{\text{II}} = \frac{E_s t}{2l_i},\ \lambda_{\text{III}} = \frac{E_s t^3}{8l_i^3}, \qquad {}^{\text{I}}\tilde{\boldsymbol{\varepsilon}} = \begin{pmatrix} 1, & 1, & 0 \end{pmatrix},\ {}^{\text{II}}\tilde{\boldsymbol{\varepsilon}} = \begin{pmatrix} 1, & -1, & 0 \end{pmatrix},\ {}^{\text{III}}\tilde{\boldsymbol{\varepsilon}} = \begin{pmatrix} 0, & 0, & 1 \end{pmatrix},$$

$$k_{\text{I}} = \frac{R_e}{E_s},\ k_{\text{II}} = \frac{R_e}{E_s},\ k_{\text{III}} = \frac{R_e}{E_s}\frac{2\sqrt{2}\ l_i}{3t}, \qquad {}^{\text{I}}\Phi_E^{\text{gr}} = \frac{R_e^2}{E_s}\frac{t}{2l_i},\ {}^{\text{II}}\Phi_E^{\text{gr}} = \frac{R_e^2}{E_s}\frac{t}{2l_i},\ {}^{\text{III}}\Phi_E^{\text{gr}} = \frac{R_e^2}{E_s}\frac{t}{9l_i},$$

$$2l_i = L$$

b) honeycomb structure

$$\mathbf{S} = \begin{bmatrix} \frac{\sqrt{3}E_s t}{6L}\frac{\left(L^2+3t^2\right)}{\left(L^2+t^2\right)} & \frac{\sqrt{3}E_s t}{6L}\frac{\left(L^2-t^2\right)}{\left(L^2+t^2\right)} & 0 \\ \frac{\sqrt{3}E_s t}{6L}\frac{\left(L^2-t^2\right)}{\left(L^2+t^2\right)} & \frac{\sqrt{3}E_s t}{6L}\frac{\left(L^2+3t^2\right)}{\left(L^2+t^2\right)} & 0 \\ 0 & 0 & \frac{\sqrt{3}E_s t^3}{3L\left(L^2+t^2\right)} \end{bmatrix}$$

$$\lambda_{\text{I}} = \frac{\sqrt{3}}{6}\frac{E_s t}{l_i}, \lambda_{\text{II}} = \lambda_{\text{III}} = \frac{\sqrt{3}}{3}\frac{E_s t^3}{l_i\left(4l_i^2+t^2\right)}, \quad {}^{\text{I}}\tilde{\boldsymbol{\varepsilon}} = \begin{pmatrix} 1, & 1, & 0 \end{pmatrix}, {}^{\text{II}}\tilde{\boldsymbol{\varepsilon}} = \begin{pmatrix} 1, & -1, & 0 \end{pmatrix}, {}^{\text{III}}\tilde{\boldsymbol{\varepsilon}} = \begin{pmatrix} 0, & 0, & 1 \end{pmatrix},$$

$$k_{\text{I}} = \frac{R_e}{E_s}, \qquad k_{\text{II}} = \frac{R_e}{E_s}\frac{\left(4l_i^2+t^2\right)}{\left(2l_i^2+t^2+3\sqrt{3}tl_i\right)}, \quad k_{\text{III}} = \frac{R_e}{E_s}\frac{\sqrt{2}\left(4l_i^2+t^2\right)}{(6l+t)t},$$

$${}^{\text{I}}\Phi_E^{\text{gr}} = \frac{R_e^2}{E_s}\frac{\sqrt{3}t}{12l_i}, \qquad {}^{\text{II}}\Phi_E^{\text{gr}} = \frac{R_e^2}{E_s}\frac{\sqrt{3}\left(4l_i^2+t^2\right)t^3}{6l_i\left(2l_i+t^2+3\sqrt{3}l_i t\right)^2}, \qquad {}^{\text{III}}\Phi_E^{\text{gr}} = \frac{R_e^2}{E_s}\frac{\sqrt{3}t}{3l_i}\frac{\left(4l_i^2+t^2\right)}{\left(6l_i+t\right)^2}$$

c) equilateral triangular structure

$$\mathbf{S} = \begin{bmatrix} \frac{\sqrt{3}E_s t\left(3L^2+2t^2\right)}{4L^3} & \frac{\sqrt{3}E_s t\left(L^2-t^2\right)}{4L^3} & 0 \\ \frac{\sqrt{3}E_s t\left(L^2-t^2\right)}{4L^3} & \frac{\sqrt{3}E_s t\left(3L^2+2t^2\right)}{4L^3} & 0 \\ 0 & 0 & \frac{\sqrt{3}E_s t}{4L} \end{bmatrix}$$

$$\lambda_{\text{I}} = \frac{\sqrt{3}}{6}\frac{E_s t}{l_i}, \lambda_{\text{II}} = \lambda_{\text{III}} = \frac{\sqrt{3}}{3}\frac{E_s t^3}{l_i\left(4l_i^2+t^2\right)}, \quad {}^{\text{I}}\tilde{\boldsymbol{\varepsilon}} = \begin{pmatrix} 1, & 1, & 0 \end{pmatrix}, {}^{\text{II}}\tilde{\boldsymbol{\varepsilon}} = \begin{pmatrix} 1, & -1, & 0 \end{pmatrix}, {}^{\text{III}}\tilde{\boldsymbol{\varepsilon}} = \begin{pmatrix} 0, & 0, & 1 \end{pmatrix},$$

$$k_{\text{I}} = \frac{R_e}{E_s}, k_{\text{II}} = \frac{R_e}{E_s}\frac{\left(4l_i^2+t^2\right)}{\left(2l_i^2+t^2+3\sqrt{3}tl_i\right)}, k_{\text{III}} = \frac{R_e}{E_s}\frac{\sqrt{2}\left(4l_i^2+t^2\right)}{(6l+t)t},$$

$${}^{\mathrm{I}}\Phi_E^{\mathrm{gr}} = \frac{R_e^2}{E_s}\frac{\sqrt{3}\left(4l_i^2+t^2\right)t}{64l_i^3}, \qquad {}^{\mathrm{II}}\Phi_E^{\mathrm{gr}} = \frac{R_e^2}{E_s}\frac{2\sqrt{3}l_i t}{\left(2l_i+3\sqrt{3}t\right)^2}, \qquad {}^{\mathrm{III}}\Phi_E^{\mathrm{gr}} = \frac{R_e^2}{E_s}\frac{\sqrt{3}l_i}{96t}$$

d) Inverted honeycomb, re-entrant structure.

$$\mathbf{S} = \begin{bmatrix} s_{1111} & s_{1122} & 0 \\ s_{1122} & s_{2222} & 0 \\ 0 & 0 & 2s_{1212} \end{bmatrix},$$

$$\lambda_{\mathrm{I}} = \frac{1}{2}\left(s_{1111}+s_{2222}-\sqrt{\left(s_{1111}-s_{2222}\right)^2+4s_{1122}^2}\right), \ \lambda_{\mathrm{II}} = \frac{1}{2}\left(s_{1111}+s_{2222}+\sqrt{\left(s_{1111}-s_{2222}\right)^2+4s_{1122}^2}\right),$$
$$\lambda_{\mathrm{III}} = 2s_{1212}$$

$${}^{\mathrm{I}}\tilde{\varepsilon}_x = 1.0, \ {}^{\mathrm{I}}\tilde{\varepsilon}_y = \frac{\left(s_{2222}-s_{1111}-\sqrt{\left(s_{1111}-s_{2222}\right)^2+4s_{1122}^2}\right)}{2s_{1122}}, \ {}^{\mathrm{I}}\tilde{\varepsilon}_{xy} = 0,$$

$${}^{\mathrm{II}}\tilde{\varepsilon}_x = 1.0, \ {}^{\mathrm{II}}\tilde{\varepsilon}_y = \frac{\left(s_{2222}-s_{1111}+\sqrt{\left(s_{1111}-s_{2222}\right)^2+4s_{1122}^2}\right)}{2s_{1122}}, \ {}^{\mathrm{II}}\tilde{\varepsilon}_{xy} = 0,$$

$${}^{\mathrm{III}}\tilde{\varepsilon}_x = 0, \ {}^{\mathrm{III}}\tilde{\varepsilon}_y = 0, \ {}^{\mathrm{I}}\tilde{\varepsilon}_{xy} = 1.0.$$

$\mathbf{S}$, $k_\alpha$, ${}^{\alpha}\Phi_E^{\mathrm{gr}}$ - obtained numerically.

**Appendix 2.**

**Macroscopic material parameters and admissible vertical pressure in uniaxial tension in dependence on the angle of tension direction.**

Skeleton material data : $E_S$=10GPa, $\nu_S$=0.3, $R_e$=10MPa,
Geometrical parameters of microstructures as given in Table 1.

a) Square cell structure (anisotropic material)

analytical formula:

$$E = \frac{E_s t^3}{L\left[t^2\left(1-\sin^2 2\alpha\right)+L^2\right]} \qquad \nu = \frac{\left(L^2-t^2\right)\sin^2 2\alpha}{\left[t^2\cos^2 2\alpha+L^2\right]}$$

$$E_{\min} = E\left(\alpha=\frac{\pi}{4}\right) = \frac{E_s t^3}{L^3} \qquad \nu_{\max} = \nu\left(\alpha=\frac{\pi}{4}\right) = \frac{\left(L^2-t^2\right)}{L^2}$$

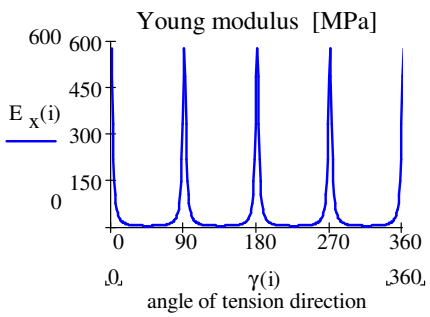


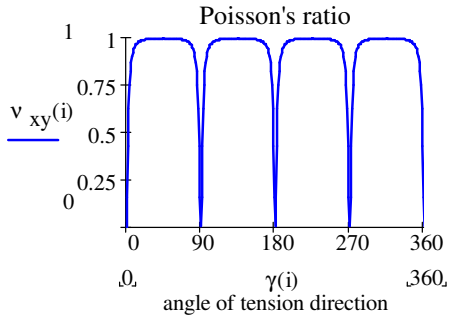


analytical formula:

$$p_{\max} = \frac{4R_e t^2}{L\left[4t^2\left(1+\cos^2 2\beta\right)+18L^2\sin^2 2\beta\right]^{1/2}}$$

Maximum of vertical load [MN/m]

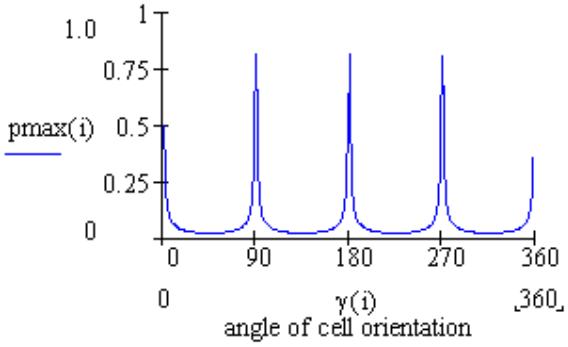


b) Honeycomb structure (isotropic material)

analytical formulae:

$$E = \frac{4E_s t^3}{\sqrt{3}L\left[3t^2+L^2\right]} = 21.87 \text{ MPa},$$

$$\nu = \frac{\left(L^2-t^2\right)}{L^2+3t^2} = 0.96, \qquad \nu_{\max} = \nu\left(\frac{t}{L}\to 0\right) = 1$$

$p_{max}$=0.3 MN/m

c) equilateral triangle cell structure (isotropic material)

analytical formulae:

$$E = \frac{\sqrt{3}E_s t\left(4L^2+t^2\right)\left(2L^2+t^2\right)}{4L^3\left[2t^2+3L^2\right]} = 385.47 \text{ MPa},$$

$$\nu = \frac{L^2-t^2}{3L^2+2t^2} = 0.33 \qquad \nu_{\max} = \nu\left(\frac{t}{L}\to 0\right) = 0.333$$

$p_{max}$=2.77MN/m

d) re-entrant structure (anisotropic material)

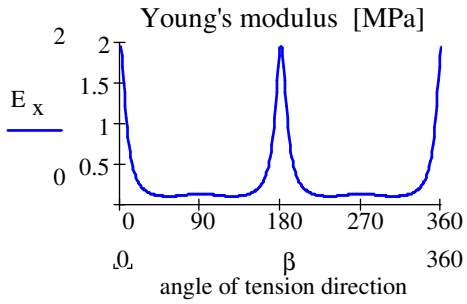


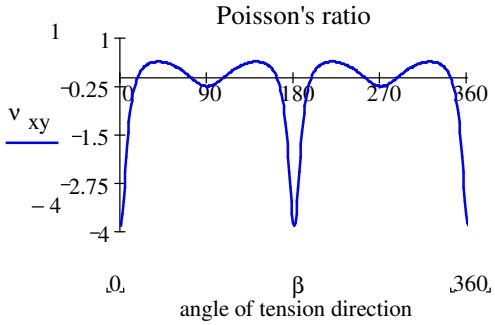


Maximum of vertical load [MN/m]

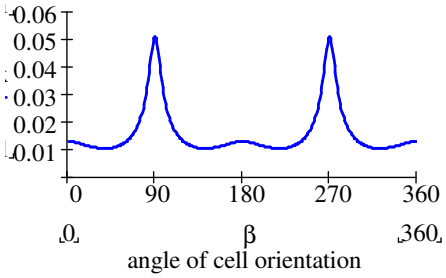


**Streszczenie**

W pracy rozważane jest płaskie zagadnienie kontaktowe sformułowane dla sprężystego ośrodka anizotropowego. Jako continuum anizotropowe o różnej symetrii materiałowej przyjęto materiały komórkowe. Rozważane są typowe struktury płaskie o szkielecie belkowym. Wśród nich wyróżniono strukturę dającą materiał o ujemnym współczynniku Poissona. Własności sprężyste materiałów komórkowych są otrzymywane jako wynik rozważań dwuskalowych opartych na modelowaniu mikromechanicznym (Ref.[2],[3]). Warunek graniczny stanu sprężystego dla materiału jest sformułowany w postaci kryterium energetycznego (Ref. [13]) stosowanego jako kryterium wytężeniowe dla dowolnych ciał anizotropowych. Wprowadzenie do analizy energetycznego współczynnika wytężenia w postaci ważonych energii zgromadzonych w stanach własnych tensora sztywności pozwala na określenie czy w zadanym stanie naprężeń materiał pracuje w zakresie sprężystym. Zagadnienie kontaktowe z tarciem jest analizowane programem MES. Obliczenia są przeprowadzone dla kwadratowego bloku obciążonego pionowym ciśnieniem wykonanego z materiału komórkowego w kontakcie z szorstkim sztywnym podłożem. Wyniki numeryczne wskazują na istotne różnice w rozkładzie naprężeń i sposobie deformacji analizowanego materiału. Szczegółowe rozważania wskazują na dobór parametrów mikrostruktury materiału zapewniającej redukcję koncentracji naprężeń w strefie kontaktu i stosowalność materiału do zadania kontaktowego z określonym typem obciążenia.